PLATFORM EFFECT REDUCTION BETWEEN ANTENNAS USING ANTENNA COUPLING SYNTHETIC APERTURE RADAR (ACSAR) IMAGING CONCEPT

Caner Özdemir
E-mail: cozdemir@mersin.edu.tr
Mersin University, Engineering Faculty, Department of Electrical & Electronics Engineering, 33342, Çiftlikköy, Mersin, Turkey

Key words: Antenna-platform interaction, radiation center model, SAR imaging

ABSTRACT

Antenna Coupling Synthetic Aperture Radar (ACSAR) imaging concept is reviewed. By using the sparseness of an ACSAR image, a radiation center representation of ACSAR imagery is obtained. Dominant point radiators are extracted from the image by using the image processing tool CLEAN to form the radiation center model of the ACSAR image. With the help of this model, a practical method of reducing the undesired antenna-platform interaction is presented. Numerical examples to demonstrate the effectiveness of this method are provided.

I. INTRODUCTION

For antennas that are mounted on a large, complex platform, the electromagnetic interaction between the antenna and the platform is inevitable as well as the direct coupling between the antennas. This secondary coupling due to platform effect is generally undesirable for most of the applications. We recently introduced new platform imaging algorithms to pinpoint the locations of secondary points off the platform [1, 2]. This kind of information is so useful to the antenna designer that he/she can utilize these algorithms in cancelling or mitigating this undesired secondary radiation.

In this work, we devise a scheme based on the Antenna Coupling Synthetic Aperture Radar (ACSAR) imaging algorithm to reduce the effect of coupling between the antennas. First, we start with a brief review of ACSAR imaging concept. Then, we continue with a sparse representation of ACSAR imagery by the scattering center model approach. This idea is motivated by the fact that ACSAR image is quite sparse since it contains mainly point radiators. By using the image-extraction tool known as CLEAN, we successfully obtained the "radiation center model" for ACSAR. This representation is quite similar to "scattering center model" that is widely-used in electromagnetic community [3-6]. Such a representation can be used to reconstruct and extrapolate antenna radiation patterns over frequencies and angles with good fidelity, thus achieving high data compression ratio. A numerical example of radiation center model is also provided to demonstrate the use of this model.

In section IV, we offer a technique for reducing the antenna-platform interaction based on the point radiator model of ACSAR imagery. Since radiation center model shows the locations of dominant point radiators off the platform, we can utilize this information to put perfect absorbers around the radiation center locations to reduce the electromagnetic scattering around these points. A numerical example that illustrates the effectiveness of our technique is demonstrated.

II. ACSAR IMAGE FORMATION

The geometry for ACSAR imaging is shown in Fig.1. In this figure, R_{1i} corresponds to the wave path from transmitter to the platform point P which we want to image. R_{2i} corresponds to the wave path from the platform point to the receiver. At the receiver site, spatial diversity on a two-dimensional aperture centered at (x_0, 0, 0) is used to achieve resolution in the two cross range dimensions y and z. The resolution in the down range or x-direction is aimed to be achieved by the diversity in frequency.

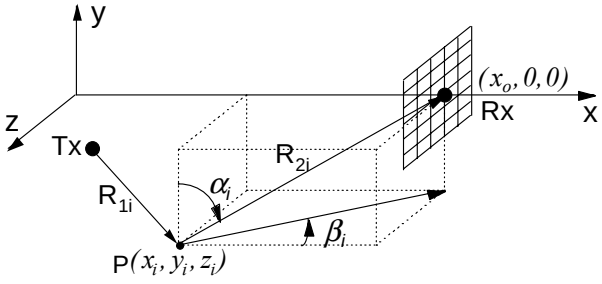

Figure 1: The geometry for ACSAR imaging.

The scattered electric field at the receiver site due to the scattering from a point P(x_i, y_i, z_i) on the platform can be written as

$$E_s(k) = A_i \cdot e^{-jkR_{1i}} \cdot e^{-jkR_{2i}} \qquad (1)$$

where A_I is the strength of the scattered field and k is the free-space wave number. Starting from equation (1) and under the small bandwidth and small aperture approximations, the ACSAR image of the point P on the platform can be found as

$$\begin{aligned} \mathrm{ACSAR(R,u,v)} &= \mathrm{IFT}\{E_s(k,y,z)\} = \mathrm{IFT}\left\{A_i \cdot e^{-jk\cdot R} \cdot e^{-jk_o\cdot u} \cdot e^{-jk_o\cdot v}\right\} \\ &= A_i \cdot \delta(R-R_i) \cdot \delta(u-u_i) \cdot \delta(v-v_i) \qquad (2) \end{aligned}$$

where $R_i = R_{1i} + R_{2i}$, $u_i = k_o \cos\alpha_i$ and $v_i = k_o \sin\alpha_i \sin\beta_i$. IFT stands for Inverse Fourier Transform operation. The detailed derivation of equation (2) can be found in [2] and will not be repeated here.

The steps required to get the ACSAR image can be summarized as

(i) Collect multi-frequency, multi-spatial platform coupling data E_S (k, y, z),
(ii) Take the 3-D inverse Fourier transform of E_S (k, y, z), to form ACSAR(R, u, v),
(iii) Use coordinate transformation formulas in [2] to get the final ACSAR(x, y, z) image in the platform coordinates.

The ACSAR image formation algorithm discussed in this section can be applied to either measurement or simulation data.

III. RADIATION CENTER MODEL

Since ACSAR image pinpoints the dominant scattering points off the platform, it is actually a sparse data set. This is because the electromagnetic rays interfere with each other to give rise to strong coherent scattering over a small, localized area on the platform. Therefore, it may be possible to represent the ACSAR image by a finite set of point radiators which we term as "radiation centers" [7]. We adopt a point radiator model of ACSAR image as follows:

$$ACSAR(x,y,z) \approx \sum_{\substack{n \text{ radiation} \\ \text{centers}}} A_n \cdot h(x-x_n, y-y_n, z-z_n) \qquad (3)$$

where $h(x,y,z) = e^{jk_o x} \sin c(\Delta k \cdot x) \cdot \sin c(\Delta y \cdot y) \cdot \sin c(\Delta z \cdot z)$ and also known as ray-spread function. Δk, Δy, and Δz are the bandwidths in wave number and aperture dimensions in y and z, respectively. k_o stands for the wave number for the center frequency and (x_n, y_n, z_n) is the location of the n^{th} radiation center.

Extraction process is done by well-known image processing tool CLEAN [8-9] which successively picks out the highest point in the image and removes its point-spread function (assumed to be the ray-spread function in this case) from the image. At the *n*th iteration of CLEAN, if the strength of the point scatterer is A_n, the 3-D residual image can be expressed as

$$\begin{aligned} \{\text{3-d Residual Image}\}_{n+1} = \{\text{3-d Residual Image}\}_n \\ -[A_n \cdot h(x-x_n, y-y_n, z-z_n)] \qquad (4) \end{aligned}$$

During each iteration, only (A_n, x_n, y_n, z_n) set needs to be stored. This iterative process continues until a user-defined threshold point is reached

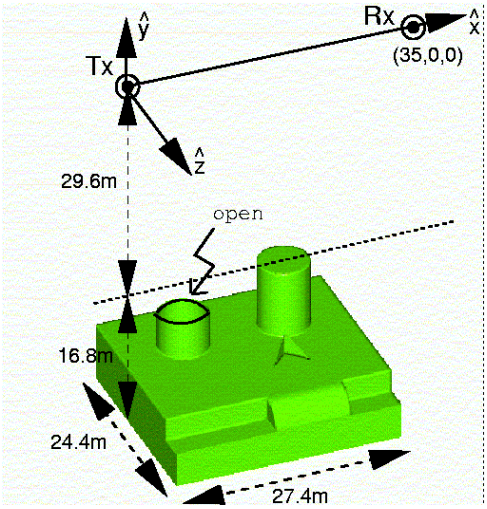

Figure 2: Test example: Slicy.

We applied the above algorithm to a test object 'Slicy' whose CAD geometry is shown in Fig.2. Slicy consists of a closed cylinder, an open cylinder, a corner reflector and a step region placed on top of a platform. All objects are assumed to be perfectly conducting. A half-wave dipole (at 10 GHz) is used as the transmitter placed at the origin. A total of 32 frequencies are computed within a 0.19 GHz bandwidth at the center frequency of 10 GHz. The simulation is carried out by a modified version of the Shooting and Bouncing Ray (SBR) code APATCH [10]. The SBR technique, first introduced by Ling, Chou and Lee, is now an accepted standard in simulating the scattering from complex targets [11-13]. The scattered field is collected on an aperture centered at (35m, 0, 0). There are 32x32=1024 spatial points on the aperture, ranging from -0.49m to 0.49m along the z direction and from -1.14m to 1.14m along the y direction. In the computed data, only the scattered field from the platform is considered and the direct radiation from the antenna is excluded. The 2-D projected ACSAR images from the 3-D ACSAR data are shown in Fig.3a. As shown in the figure, the dominant scattering is from the middle of the platform around the point (17.5m, -40m, 0). This is the

expected specular point on the platform. We also see other dominant scattering points corresponding to different scattering features. Next, we employ the extraction routine to extract a total of 150 radiation centers from the image using the scheme explained above. The locations of these radiation centers are depicted in Fig.3b. Then, to see the effectiveness of our model, we reconstruct the image using the extracted radiation centers by applying formula (3). The reconstructed image is shown in Fig.3c. The agreement between Fig.3a and Fig.3c proves the strength of our sparse set of radiation center model.

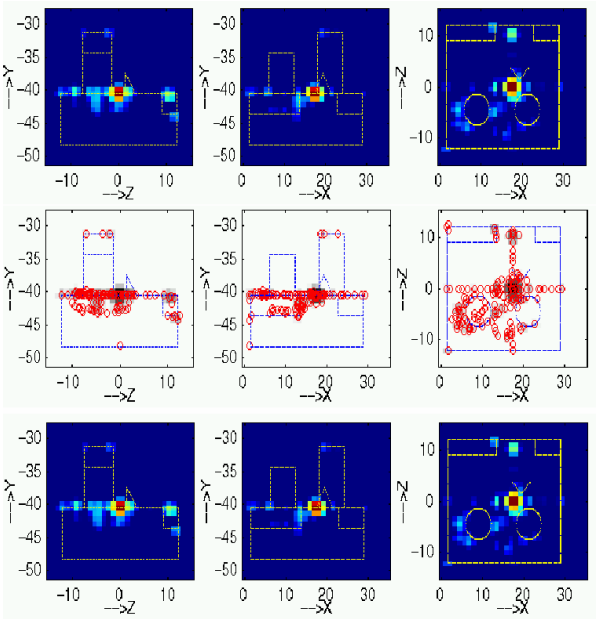

Figure 3. (a) (Top three figures) 2-D projected ACSAR images obtained by APATCH simulation and the ACSAR imaging algorithm. (b) (Middle three figures) The locations of the 150 extracted radiation centers. (c) (Bottom three figures) 2-D projected ACSAR images reconstructed by using the extracted radiation centers.

IV. PLATFORM EFFECT REDUCTION

In this section, we shall demonstrate an application of the radiation center model. Since the radiation centers pinpoint the locations of the dominant secondary scattering on the platform, one way to mitigate such undesirable effects is by placing absorbers around those locations. Therefore, the radiation from those locations can be blocked out to reduce the platform coupling between the transmitter and the receiver.

The same numerical example in the previous section is used for our demonstration of platform effect reduction study. We only consider the first 50 radiation centers from the radiation center data set to use them in our platform-reduction scheme. The reason of stopping at 50th radiation center can be explained with Fig. 4. This figure shows the normalized magnitudes of the radiation centers extracted from the ACSAR image in Fig.3 versus the radiation center number. As seen from the figure, the normalized amplitudes are levelled around -20dB after 50th to 60th radiation center. In fact, the amplitude of the 50th radiation center is -18.4dB. Therefore, in order to keep the number of the facets to be converted into absorbers small while achieving a good reduction of the scattered field, 50 seems to be a good number to be compromised.

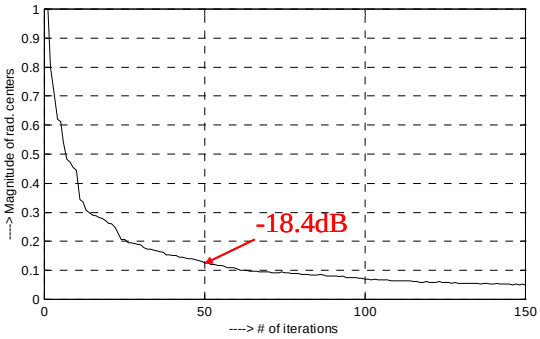

Figure 4. The normalized magnitudes of the extracted radiation centers.

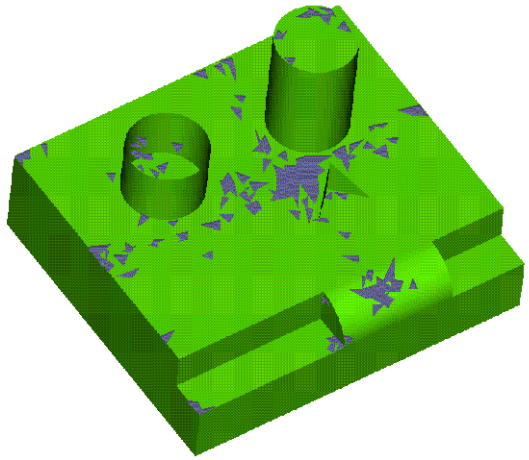

Figure 5. The modified CAD file of Slicy with absorbing facets shown darker.

In the next step, we directly go to the CAD file of Slicy to convert those perfect electric conducting (PEC) facets that are close to those 50 radiation center locations to perfect absorbers. During this process, we have converted only 353 facets to perfect absorbers out of approximately 34,000 facets that form the whole geometry for Slicy. The new CAD file with absorbers placed on different radiation center locations can be seen in Fig.5. The facets that are converted into absorbers are shown with darker colour. As the last step, we simulated the new CAD file with APATCH code to observe the amount of reduction in platform scattering due to the absorbers on the platform. The old and new ACSAR images corresponding to the cases with and without absorbers are shown in Fig.6a, and Fig.6b, respectively. We can see the reduction effect of

absorbers in Fig.6b as the reduced image magnitude. The amplitude of the maximum image level is around -20 dB as we expected. This is because of the fact that we used the radiation centers whose magnitudes are -18.4dB or more. Therefore, all of the remaining radiation centers contribute the ACSAR image with a magnitude less than that amount.

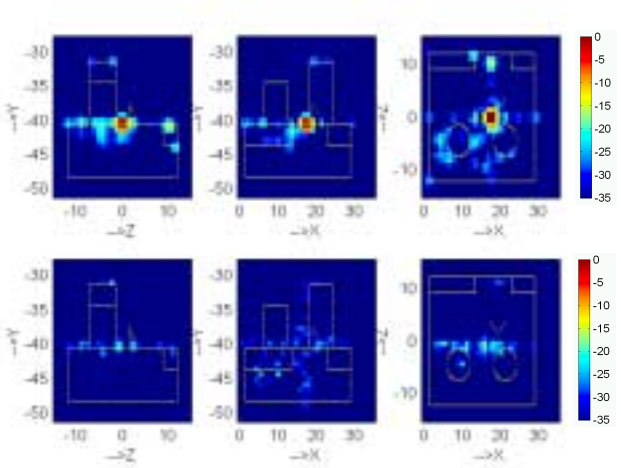

Figure 6. 2-D projected ACSAR images for Slicy (a) (Top three figures) without absorbers, (b) (Bottom three figures) with absorbers.

V. CONCLUSION

In this work, we presented a scheme that is specially tailored to radiation center model of ACSAR imaging to mitigate the platform effect. First, we reviewed the ACSAR imaging algorithm. Then, we introduced the radiation center model to sparsely represent the ACSAR image. We have shown that only a finite set of point radiators is sufficient to represent the actual image. We have also demonstrated that we can reconstruct the ACSAR image with a high fidelity by using a numerical example. As a useful application of the radiation center model, we have demonstrated that we can utilize this model to reduce the undesired platform coupling.

REFERENCES

1. C. Ozdemir, R. Bhalla, L. C. Trintinalia, and H. Ling, "ASAR - Antenna synthetic aperture radar imaging," *IEEE Trans. on Antennas and Propagat.*, vol. AP-46, pp. 1845-1852, Dec. 1998.
2. C. Ozdemir and H. Ling," ACSAR – Antenna coupling synthetic aperture radar imaging algorithm" *Journ. Electromagn. Waves Applicat.*, pp. 285-306, vol. 13, No. 3, Mar. 1999.
3. W. P. Yu, L. G. To, and K. Oii, "N-point scatterer model RCS/glint reconstruction from high-resolution ISAR target imaging," *Proc. End Game Mesa. Modelling Conf.*, pp. 197-212, Point Mugu, CA, Jan. 1991.
4. N. Y. Tseng and W. D. Burnside, "A very efficient RCS data compression and reconstruction technique," Tech. Rept. No. 722780-4, ElectroScience Lab, Ohio State Univ., Nov. 1992.
5. S. Y. Wang and S. K. Jeng, "Generation of point scatterer models using PTD/SBR technique," *IEEE Antennas Propagat. Symp. Dig.,* Newport Beach, CA, June 1995, pp. 1914-1917.
6. R. Bhalla, and H. Ling, "Three-dimensional scattering center representation using the shooting and bouncing ray technique," *IEEE Trans. on Antennas and Propagat.*, vol. AP-44, pp. 1445-1453, Nov. 1996.
7. C. Özdemir, R. Bhalla and H. Ling, "A Radiation Center Representation of Antenna Radiation Patterns on a Complex Platform," *IEEE Trans. on Antennas and Propagat.*, vol. AP-48, pp. 992-1000, No. 6, June 2000.
8. A. Selalovitz and B. D. Frieden, "A 'CLEAN'-type deconvolution algorithm," *Astron. Astrophys.*, vol. 70, pp. 335-343, 1978.
9. J. Tsao and B. D. Steinberg, "Reduction of sidelobe and speckle artifacts in microwave imaging: the CLEAN technique," *IEEE Trans. Antennas Propagat.*, vol. AP-36, pp. 543-556, Apr. 1988.
10. S. W. Lee, "Users manual for *APATCH*," version 1.0, DEMACO, Inc., Champaign, IL, Oct. 1992.
11. H. Ling, R. Chou and S. W. Lee, "Shooting and bouncing rays: calculating the RCS of an arbitrary shaped cavity," *IEEE Trans. Antennas Propagat*., vol. AP-37, pp.194-205, Feb. 1989.
12. S. W. Lee, H. Ling and R. Chou, "Ray tube integration in shooting and bouncing ray method," *Microwave Opt. Tech. Lett.,* vol.1, pp 286-289, Oct. 1988.
13. S. K. Jeng, "Near-field scattering by physical theory of diffraction and shooting and bouncing rays," *IEEE Trans. Antennas Propagat.*, vol. AP-46, pp. 551-558, April 1998.